FTS

SIGNAL-TO-NOISE

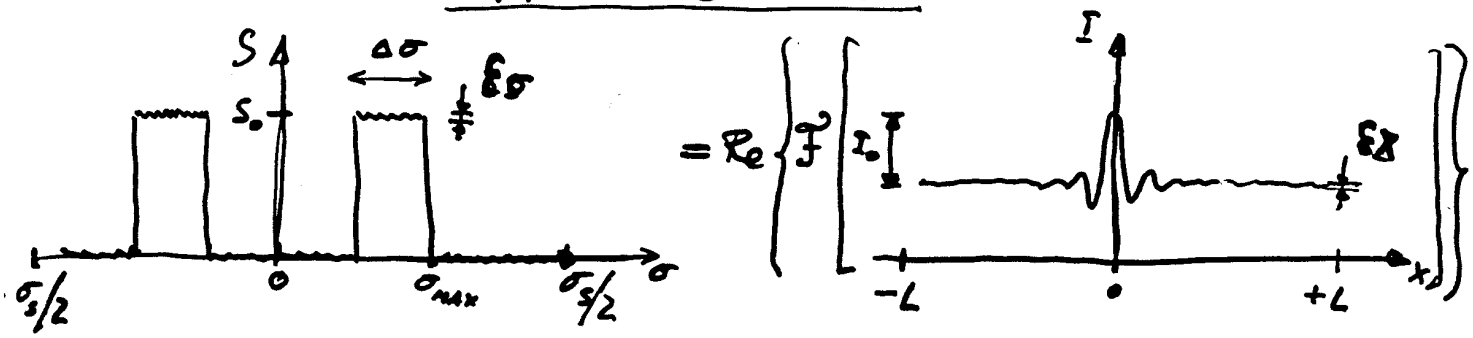

$$SNR_\sigma = \frac{S_0}{\delta\sigma} \qquad SNR_x = \frac{I_0}{\delta x}$$

- AREA THEOREM: $I_0 = 2 S_0 \Delta\sigma$
- PARSEVAL THEOREM: $\int \text{noise power}\, d\sigma = \int \text{noise power}\, dx$

(S: complex Fourier; I)

$$\Rightarrow 2\,\sigma_s\,\delta\sigma^2 = 2L\,\delta x^2$$

(2: account for imaging part; $\delta\sigma^2$: noise in real part)

$$\Rightarrow \delta\sigma = \delta x \sqrt{\frac{L}{\sigma_s}}$$

- Hence SNR:

$$SNR_\sigma = SNR_x \frac{1}{2\Delta\sigma} \sqrt{\frac{\sigma_s}{L}}$$

- Sampling at freq. σ_s requires oversampling:

$$\sigma_s = \eta\, \sigma_{MAX} \qquad \eta \geq 2 \text{ for NYQUIST}$$

$$\rightarrow \boxed{SNR_\sigma = SNR_x \frac{1}{2\Delta\sigma} \sqrt{\frac{\sigma_{MAX}\,\eta}{L}}}$$

- Valid for any vaguely bell shaped function:

SPIRE BAND I

SINGLE-PASS SNR

- Consider telescope background only
- Detector noise only, $NEP = 3 \cdot 10^{-17}\ W/\sqrt{Hz}$
- Assume $\Delta\sigma = 20\ cm^{-1}$ centred @ $40\ cm^{-1} = \sigma_0$
  $T_{tel} = 80\ K$, $\varepsilon_{tel} = 4\%$
- Take pixel size (square) $\frac{\lambda_{min}}{2D}$

$$\rightarrow P \doteq 2.3 \cdot 10^{-13}\ W/cm$$

$$SNR_x = \frac{P \Delta\sigma}{NEP\sqrt{f}} \qquad f = 20\ Hz$$

$$= 3.4 \cdot 10^4$$

- Hence: $SNR_\sigma = \frac{SNR_x}{2\Delta\sigma}\sqrt{\frac{\sigma_{MAX}\,\eta}{L}}$

$\sigma_{MAX} = 50\ cm^{-1}$
$\eta = 2$
$L = 12.5\ cm$

$$= 2400$$

- Can we gain by increasing η?
  → more spectrum?
- Co-adding increases SNR by $\sqrt{N}$
- Need to ensure sampling error gives $SNR_\sigma \gg 2400$

→ **GOAL : 10 000**

Dec 98 ©

SAMPLING ERRORS

$$\delta I = \frac{dI}{dx}\,\delta x(x) \qquad \delta x(x) \text{ is sampling error}$$

Bell-shaped spectrum, FWHM $\Delta\sigma$ centered at σ_0

$$S = S_0 e^{-4\ln 2\left(\frac{\sigma-\sigma_0}{\Delta\sigma}\right)^2}$$

Interferogram: (large steps, small steps)

$$I = I_0 \cos 2\pi\sigma_0 x \; e^{-4\ln 2\left(\frac{x}{\Delta x}\right)^2}$$

where $\Delta x = \frac{4\ln 2}{\pi\Delta\sigma} = \frac{0.88}{\Delta\sigma} \sim \frac{1}{\Delta\sigma}$

Hence: $\frac{dI}{dx} \approx I_0\, 2\pi\sigma_0 \sin 2\pi\sigma_0 x \; e^{-4\ln 2(x\Delta\sigma)^2}$

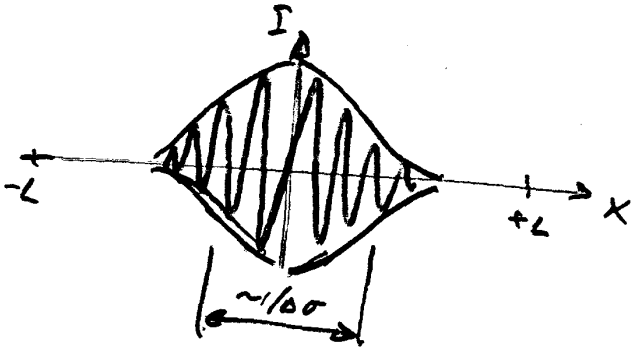

RMS noise in interferogram:

$$\varepsilon_x = I_0\,\delta x\, 2\pi\sigma_0 \frac{1}{\sqrt{2}} \sqrt{\frac{\Delta x}{2L}} \qquad \rightarrow SNR_x = \frac{I_0}{\varepsilon_x} = \frac{\sqrt{L\Delta\sigma}}{\pi}\frac{\lambda_0}{\delta x}$$

- δx: RMS of sampling error
- $\frac{1}{\sqrt{2}}$: sine modulation
- $\sqrt{\frac{\Delta x}{2L}}$: envelope

Spectral noise:

$$SNR_\sigma = \frac{I_0}{\varepsilon_\sigma} = \frac{SNR_x}{2\Delta\sigma}\sqrt{\frac{\sigma_{max}\,\eta}{L}} = \frac{1}{2\pi}\sqrt{\frac{\sigma_{max}\,\eta}{\Delta\sigma}}\,\frac{\lambda_0}{\delta x}$$

$\sigma_{MAX} = 50\ cm^{-1}$
$\eta = 4$
$\Delta\sigma = 20\ cm^{-1}$
$\lambda_0 = 2.50\ \mu m$
$\delta x = 0.5\ \mu m$

$$\boxed{SNR_\sigma = 250} \rightarrow \frac{1}{40} \text{ of goal of } 10\,000$$

Dec 98 ☺

IMPROVING THE SNR

- Increase oversampling η
  → $\eta = 16 \Rightarrow SNR_\sigma = 500$
- Reduce sampling error δx
  → Fine sampling
  → Servo loop
  → Mechanical inertia
- Reduce signal level.
  → Reference source
  → Need :

$$\frac{I_{Tel} - I_{Ref}}{I_{Tel}} \leq \frac{1}{40} = 2.5\%$$

→ 3B gives: $\boxed{\begin{array}{l} \delta T \sim 0.5\,K \\ \dfrac{\delta \varepsilon}{\varepsilon} \sim 0.1 \end{array}} \rightarrow \varepsilon' = 4\%\,,\ T' = 75\,K$

- High-pass filtering of the spectrum
  → Loss of Low R info
  → Strongly dependent upon optical filter shape

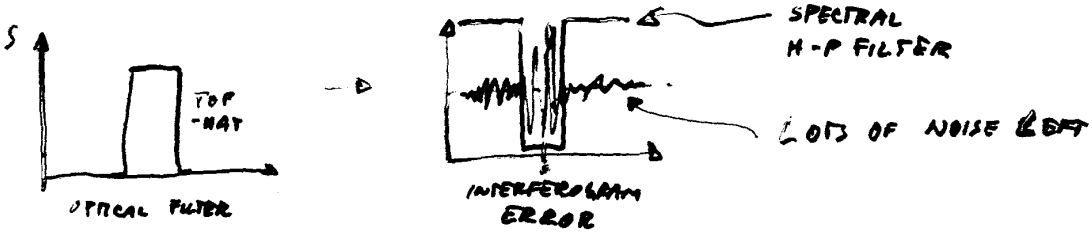

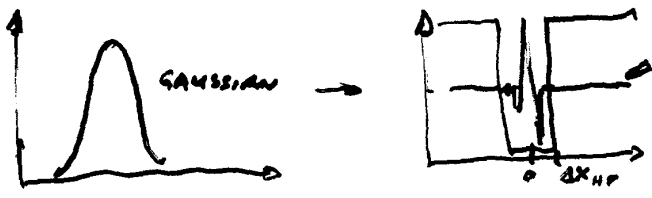

$\Delta x_{HP} = 0.075$ cm $\Rightarrow 13\,cm^{-1} \Rightarrow R_{MIN} = \frac{40}{13} = 3 \Rightarrow$

TOP-HAT	0.3
COS BELL	0.005
GAUSSIAN	0.0003

Oz 98

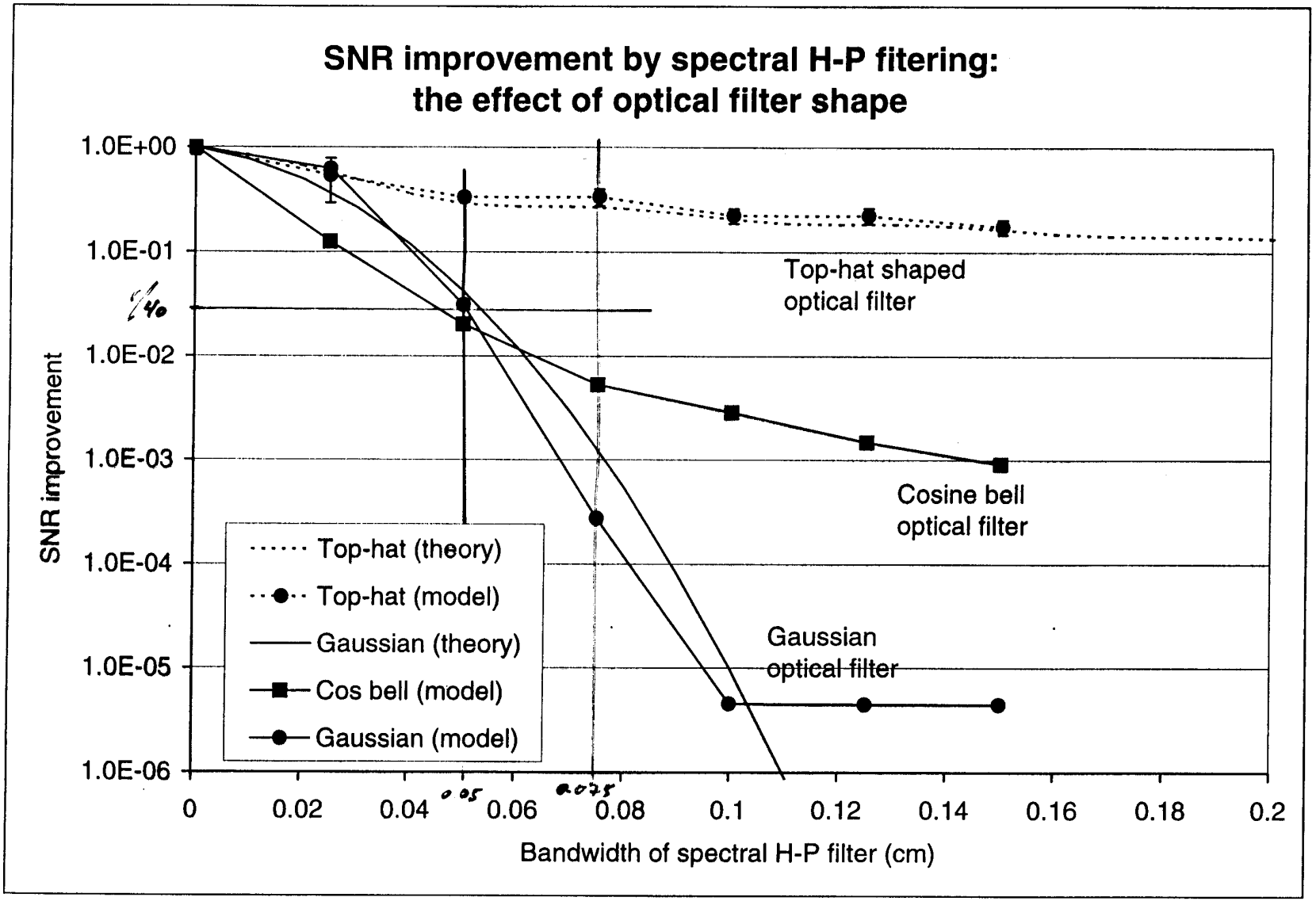
SNR improvement by spectral H-P fitering:
the effect of optical filter shape
1.0E+00
1.0E-01
1.0E-02
1.0E-03
1.0E-04
1.0E-05
1.0E-06
SNR improvement
1/40
Top-hat shaped
optical filter
Cosine bell
optical filter
Gaussian
optical filter
Top-hat (theory)
Top-hat (model)
Gaussian (theory)
Cos bell (model)
Gaussian (model)
0
0.02
0.04
0.05
0.06
0.075
0.08
0.1
0.12
0.14
0.16
0.18
0.2
Bandwidth of spectral H-P filter (cm)

TOP-HAT OPTICAL FILTER

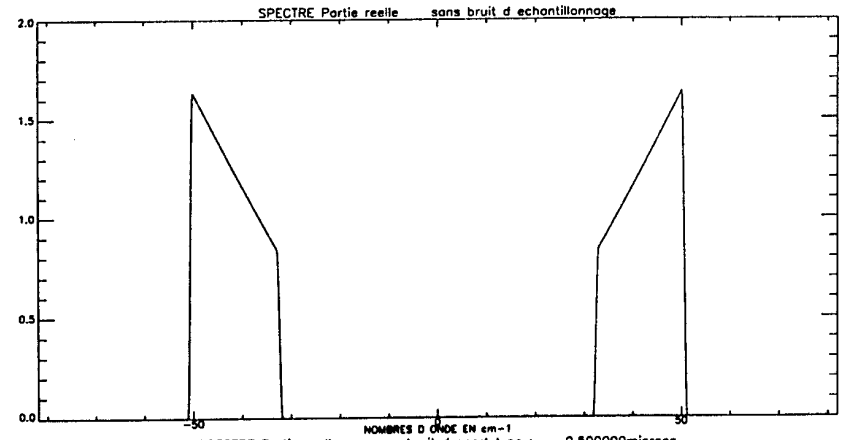

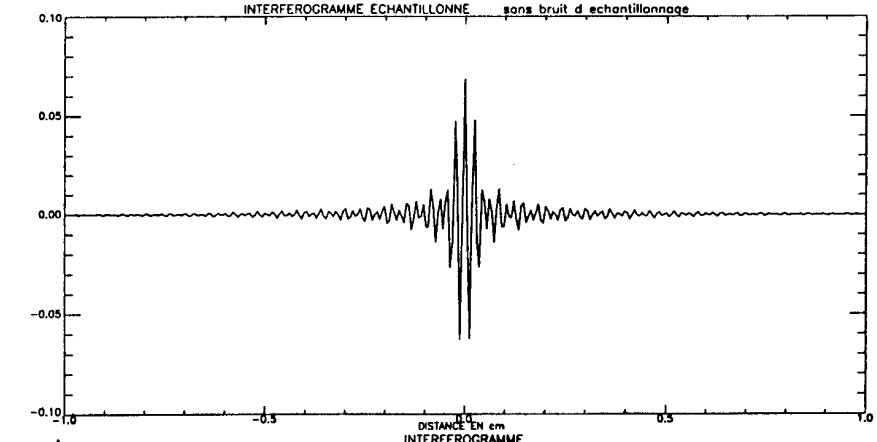

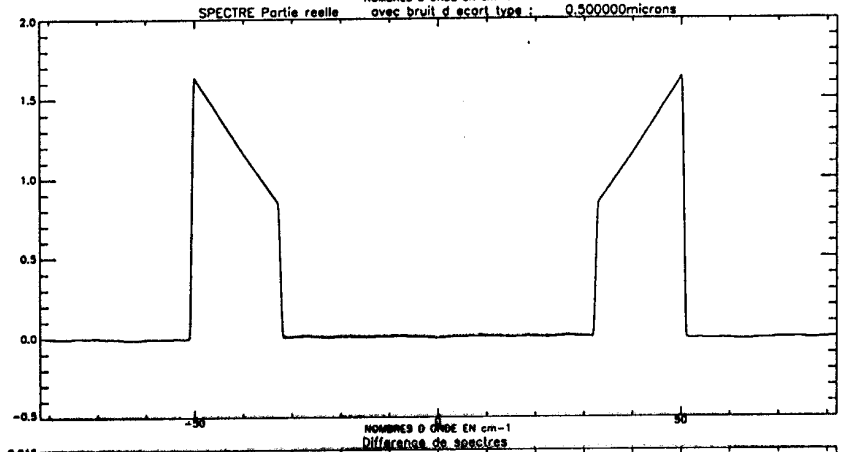

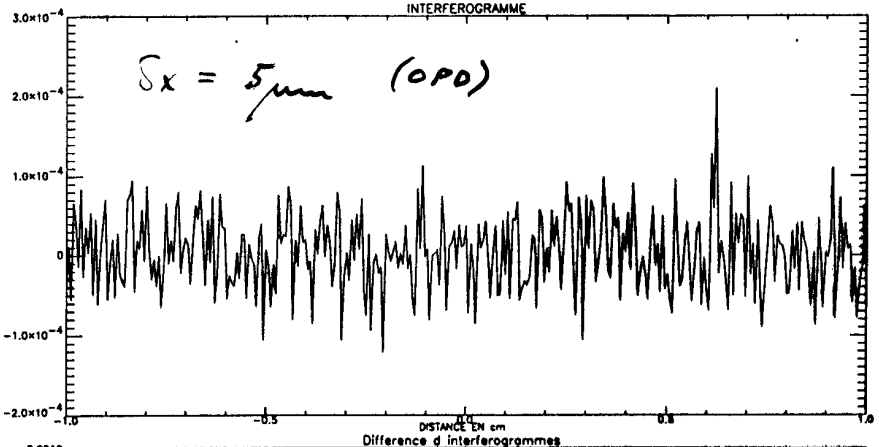

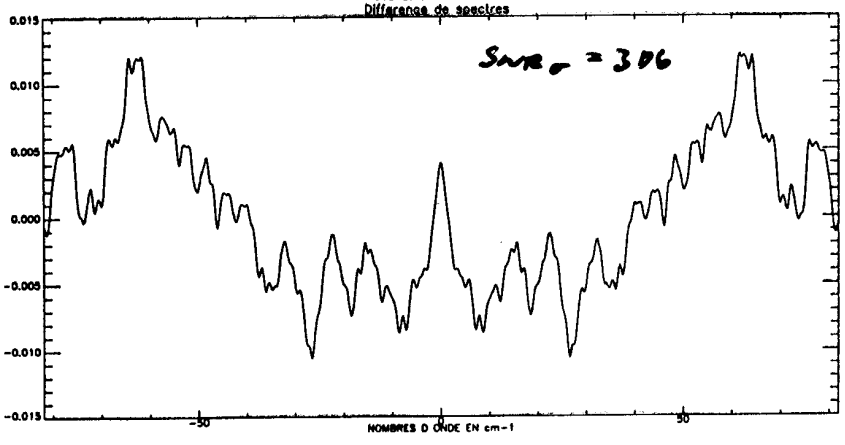

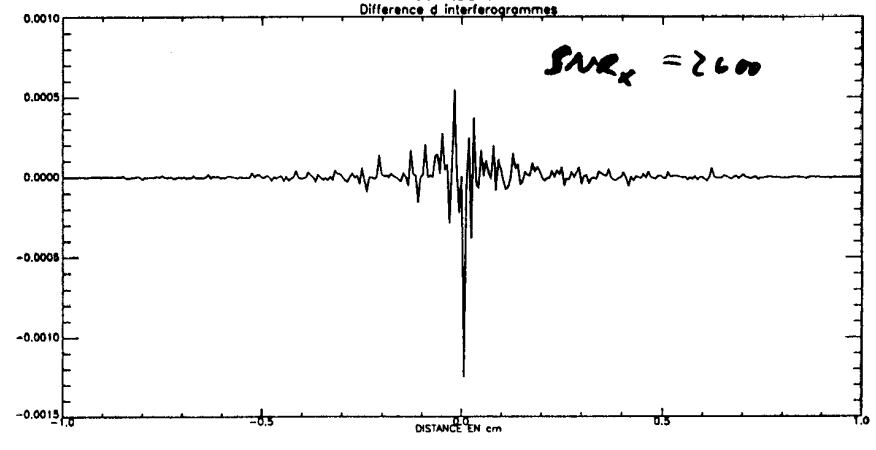

TOP-HAT OPTICAL FILTER

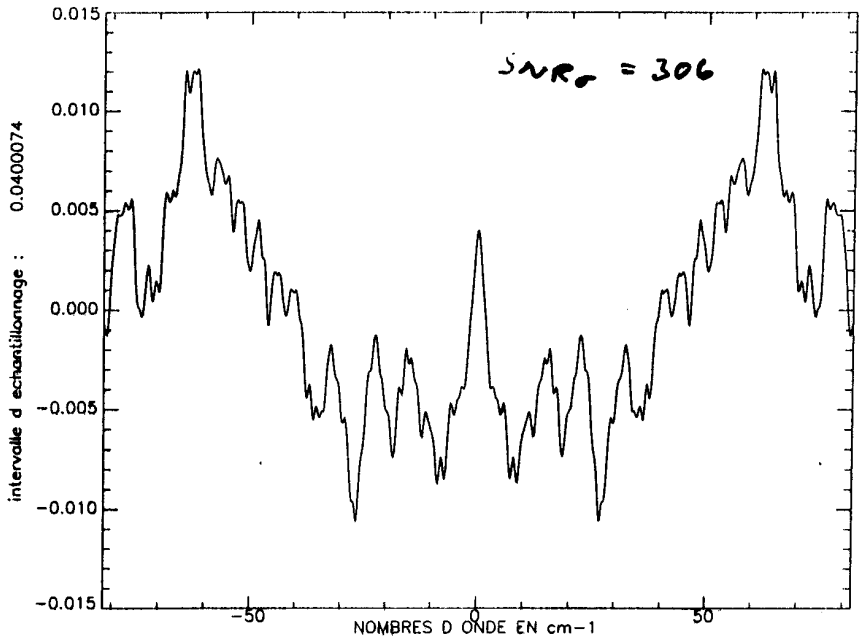

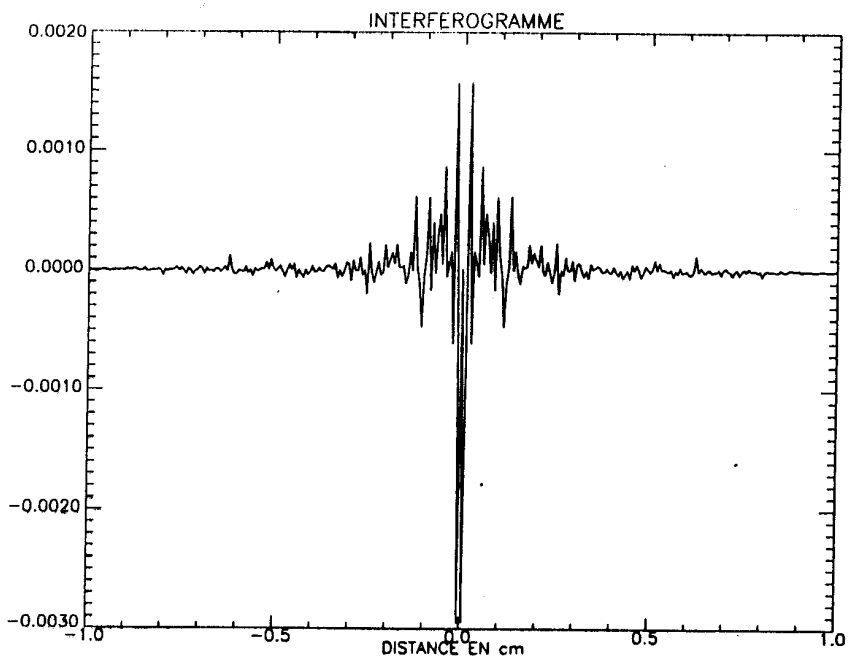

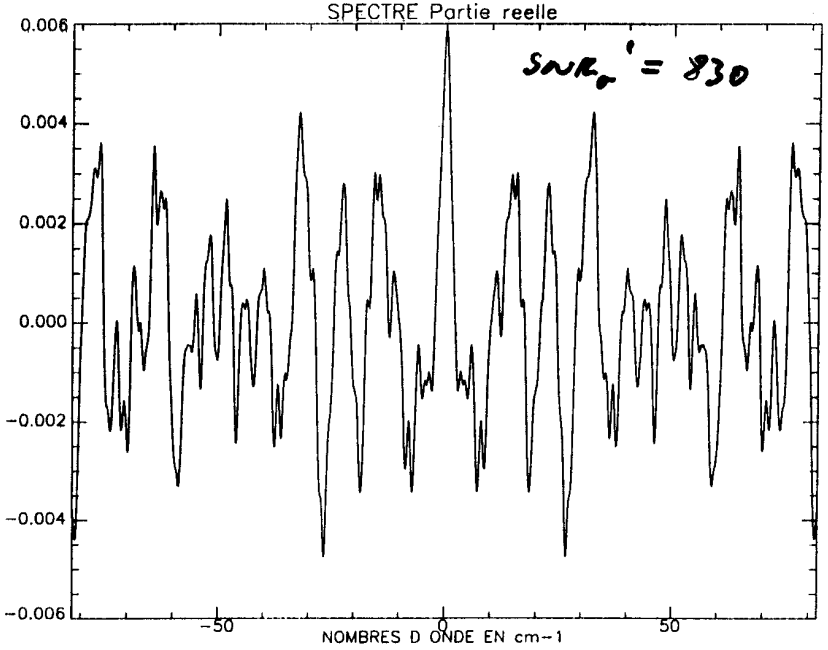

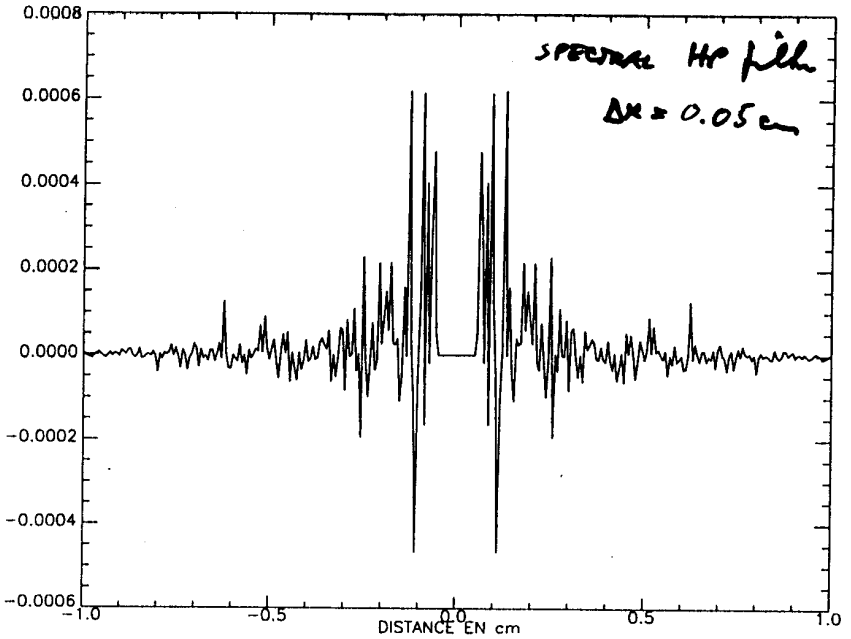

GAUSSIAN OPTICAL FILTER

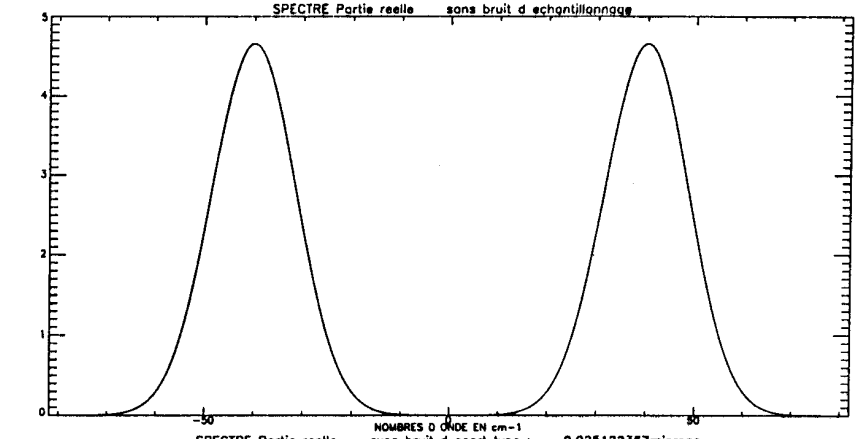

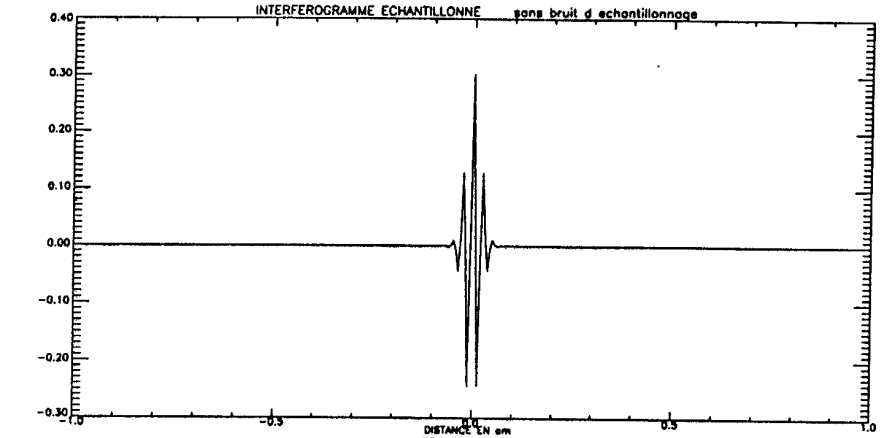

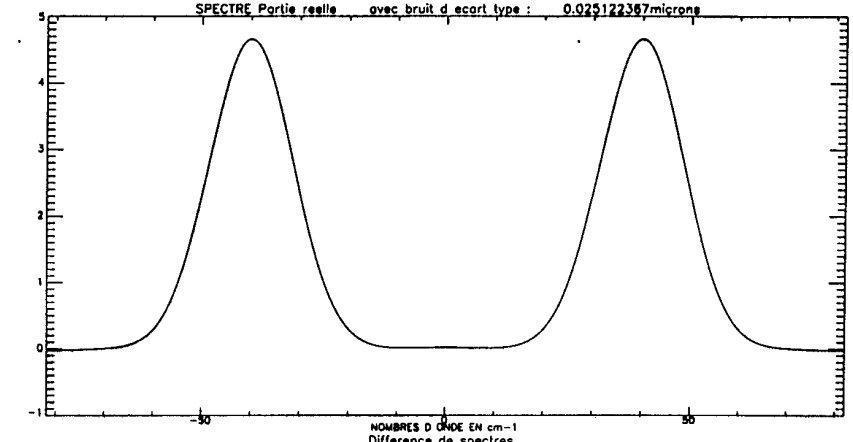

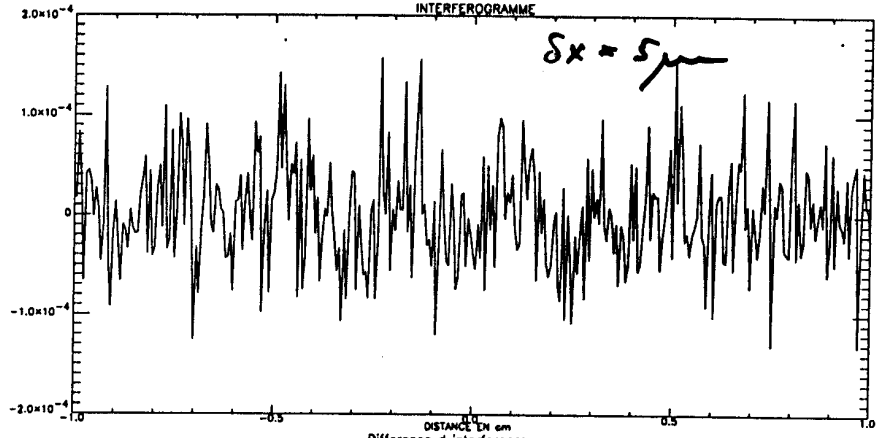

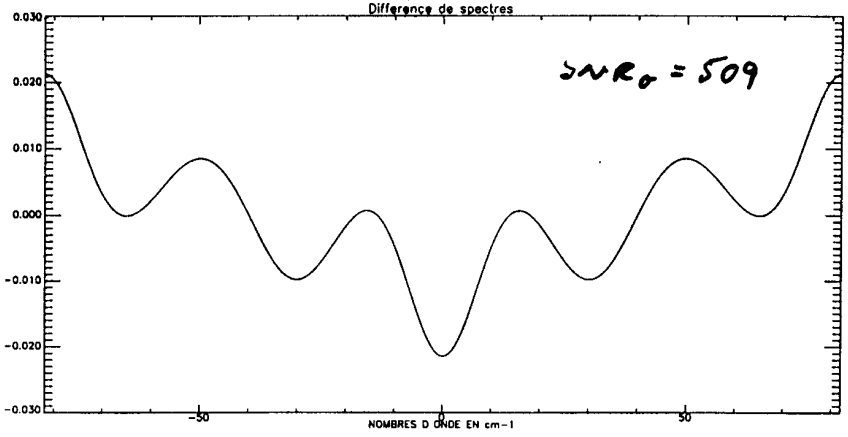

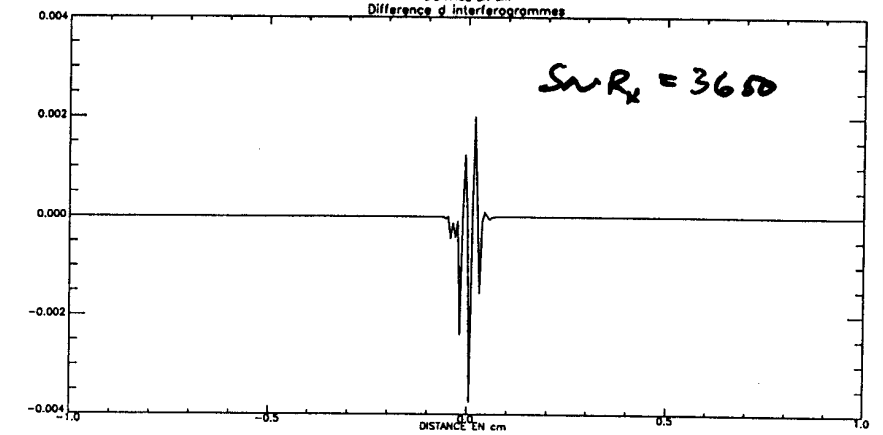

GAUSSIAN OPTICAL FILTER

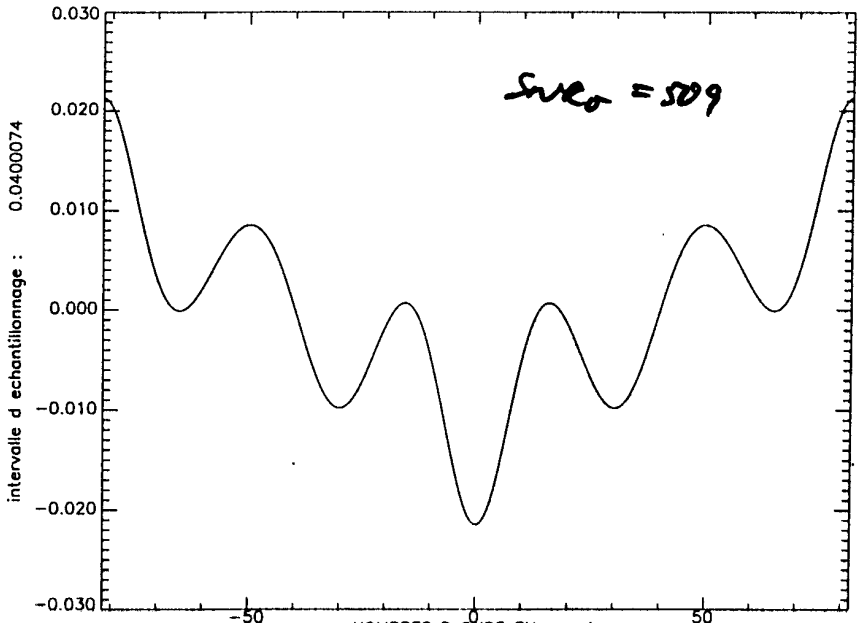

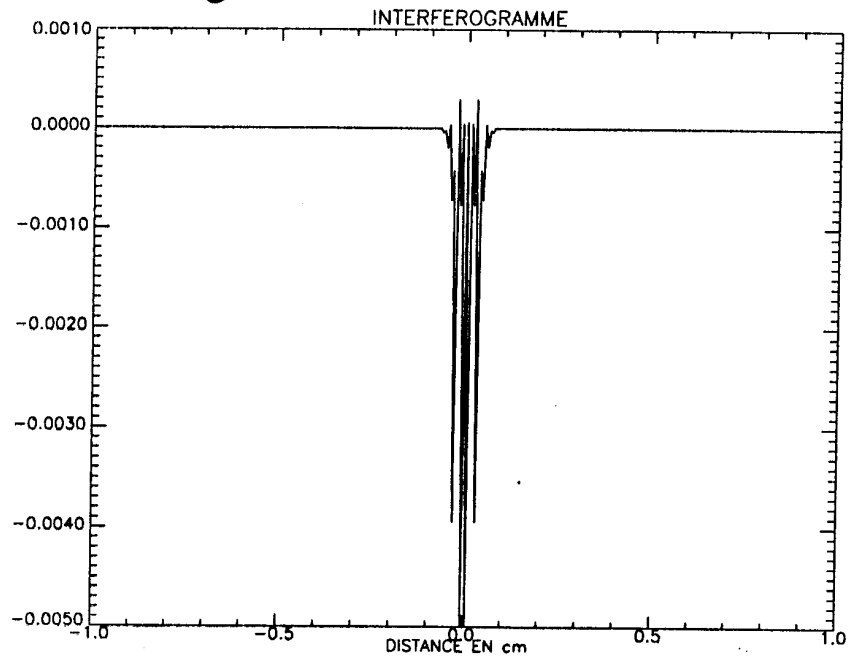

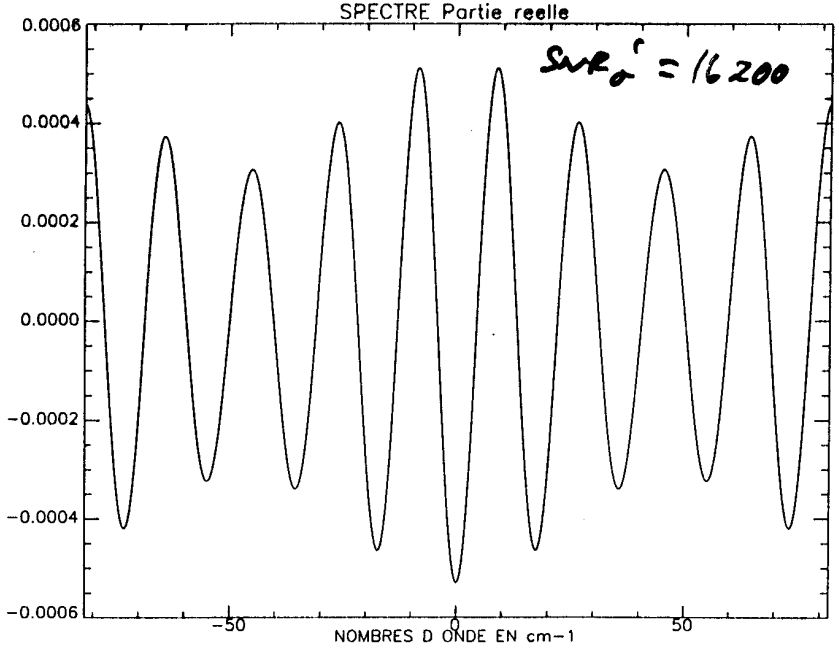

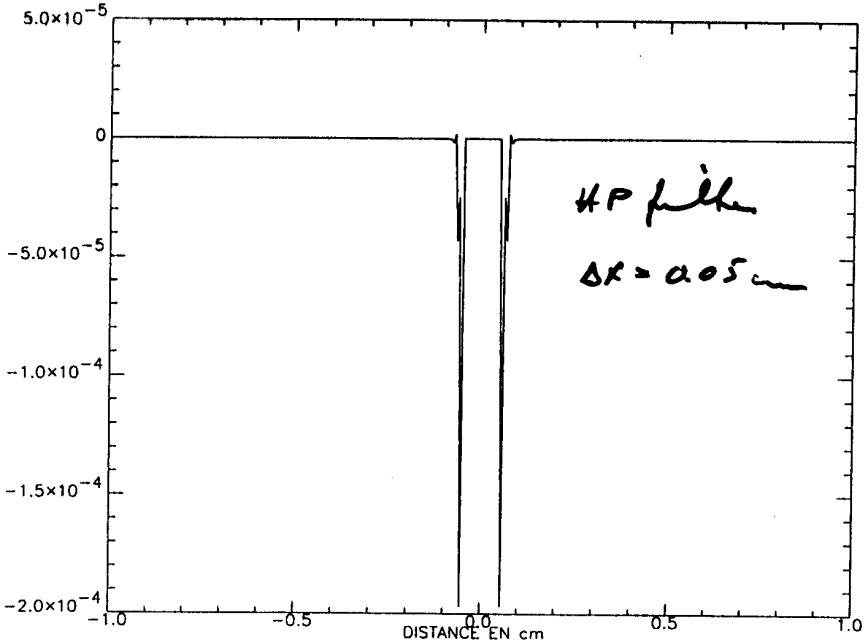

FIRST-SPIRE

New proposal for photometer optical design

Kjetil Dohlen

dohlen@observatoire.cnrs-mrs-fr

Laboratoire d'Optique, Observatoire de Marseille
2 Place Le Verrier, 13248 Marseille Cedex 4, France

1. Introduction

The original photometer proposed for SPIRE is reviewed and a different design is proposed, offering improved image and pupil quality. This is achieved at the cost of surface complexity and the appearance of distortion and variable focal ratio. The overall geometry of the system up until the cold stop is largely conserved.

2. Design criteria

We consider here design criteria concerning optical quality. Stray-light, beam clipping, thermal aspects and mechanical implementation are not considered.

Three optical design criteria may be defined:

1) **Final image quality:** We assume the Marechal criterion for diffraction limited optics, i.e. Strehl ratio $S > 0.8$ ($S = 1$ for perfect optics). This corresponds to an RMS wavefront error at $\lambda = 200$ μm of $w = \lambda/13 = 15$ μm. An error budget must be created taking into account the theoretical image quality of the instrument, FIRST telescope quality, manufacturing and alignment tolerances, etc. This has not been done for SPIRE yet. As a reasonable target for instrument optical quality we assume **$w < \lambda/20 = 10$ μm.**

2) **Intermediate image quality:** Since the spectrometer does not work in the same plane as the photometer, it is very unlikely that aberrations present in the intermediate focal plane can be corrected by the spectrometer optics. For a diffraction limited spectrometer image, the intermediate image must therefore be better than the final image, say **$w < 8$ μm.**

3) **Pupil image quality in the cold-stop:** The cold stop avoids detectors to see anything outside the telescope pupil. If the image of the pupil onto the cold stop suffers from aberrations, the pupil image is not the same for all points in the FOV. For the cold-stop to be efficient, it must then be undersized, producing a loss of signal. Again an error budget is required to take account of all the effects affecting this performance (diffraction, alignment, etc). For the present purposes we assume a requirement for the geometrical optical design of **< 10% loss of flux at the cold stop.**

3. Original design

The original design (Figure 1) uses a spherical tertiary (M3) to image the FIRST pupil (M2) onto a flat chopping mirror (M4). The chopper allows the instrument FOV to be swept across the telescope focal plane. A toroidal M5 reimages the focal plane onto an intermediate image in which is located a small pick-off mirror feeding the spectrometer channel. M5 also produces an image of the pupil, located just after the flat M6. The cold stop, materializing the limiting aperture for the instrument, is located in this pupil image. A toroidal M7 relays the star-space image onto the final focal plane, providing sufficient back-focal clearance to fit two dichroics mounted at 25° to the beam, thus feeding three individual detector arrays.

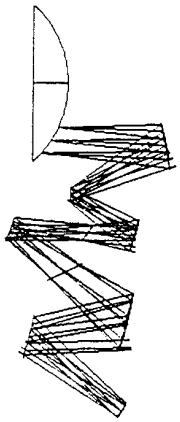

Figure 1. Present baseline design for the SPIRE photometer.

Final image quality is limited by the toroidal M7 which produces a nearly perfect image at the centre of the field but suffers from astigmatism at the edges (Figure 2 (a)). In the worst corner of a 5′ x 5′ FOV, **the wavefront error is 32 μm rms.** The specified 10 μm is achieved within a circle of diameter 3′.

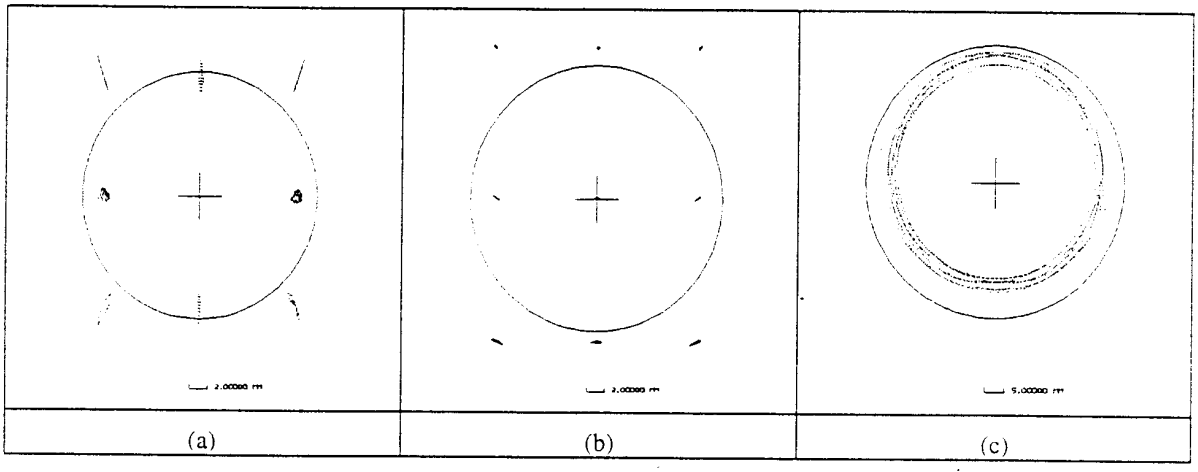

Figure 2. Raytracing results for the present baseline. (a): Final image spot diagrams for a 5′ x 5′ FOV. (b): Intermediate image spot diagrams. (c): Outline of the telescope pupil imaged onto the cold stop for several points in the field.

Image quality in the **intermediate focus** is within the specified **8 μm rms wavefront error** (Figure 2(b)). The image plane is tilted 35° wrt optical axis.

Pupil imaging suffers from coma, producing an important blurring of the image of M2 upon the cold stop (Figure 2(c)). The walk of the M2 image in the cold-stop plane is about 5 mm and the diameter of the image is about 55 mm. The cold stop must therefore be reduced to a diameter of 50 mm to avoid leakage, hence inflicting a **light loss of 17%**.

4. New proposal

We realized that pupil imaging was improved by changing M3 into an off-axis parabola, creating nearly optimal imaging of the telescope pupil onto M4. Adjusting the toricity of M5 slightly ensured a good pupil image also in the cold-stop plane (Figure 4(c)), achieving a **light loss due to pupil undersizing of about 8%**. A loss of final image quality was observed, however. Replacing the flat M6 and toroidal M7 by a couple of off-axis paraboloids with a collimated beam between them (Figure 3) was found to preserve the good pupil image while giving excellent quality in the final image (Figure 4(a)) with **RMS wavefront errors less than 8 μm**. The intermediate image quality (Figure 4(b)) is still suffichient but its tilt is increased to about 50°. This increase in tilt appears to be due to the use of a parabolic M3. Its impact upon image quality in the spectrometer has not been assessed.

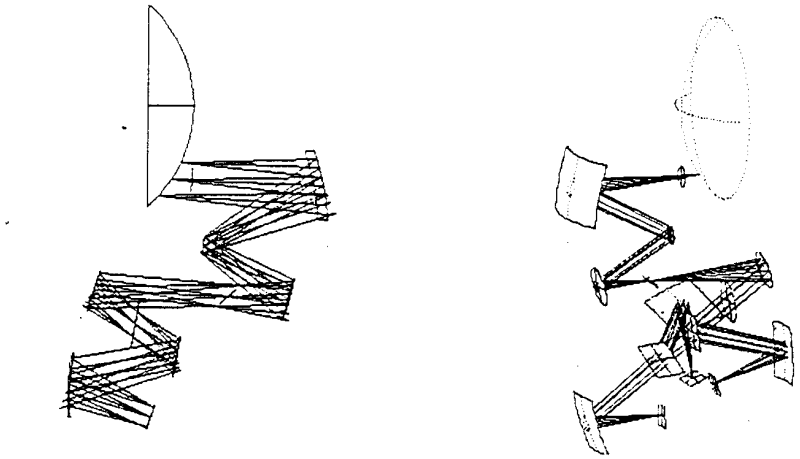

(a) (b)

Figure 3. Proposed design for the SPIRE photometer. (a): Profile drawing with a single channel. (b): Perspective drawing with all three channels.

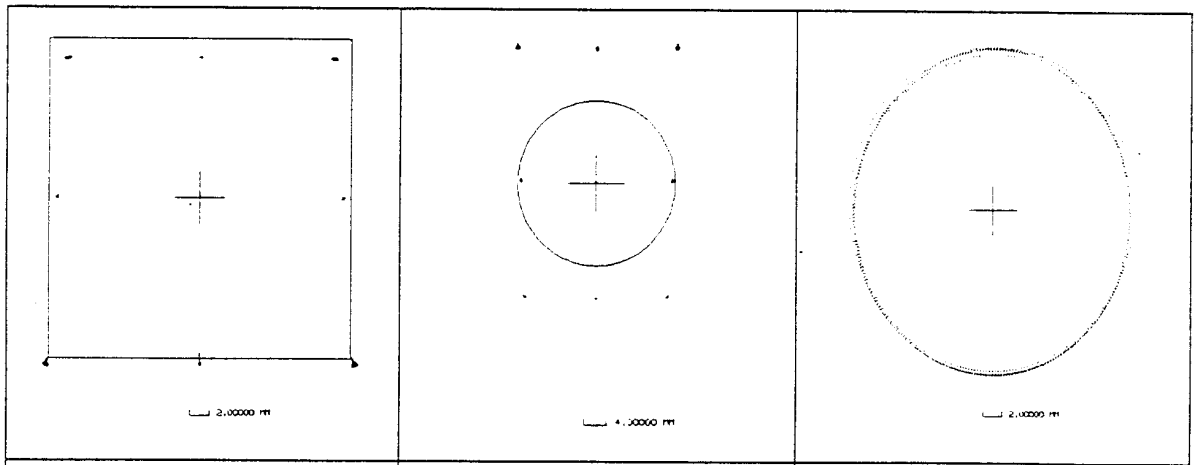

(a) (b) (c)

Figure 4. Raytracing results for the proposed design. (a): Final image spot diagrams for a 5′ x 5′ FOV. (b): Intermediate image spot diagrams. (c): Outline of the telescope pupil imaged onto the cold stop for several points in the field.

The main difference wrt the original design is that dichroics are located before rather than after M7. Each channel therefore has its own (parabolic) M7 focalizing the beam onto the detector arrays. The dichroics are mounted at 25° to the beam and one of them send the beam out into the plane perpendicular to the plane of the system. Figure 3(b) shows a 3D view of the complete system. The focal planes are located on three sides of an approximately rectangular box as indicated in Figure 5.

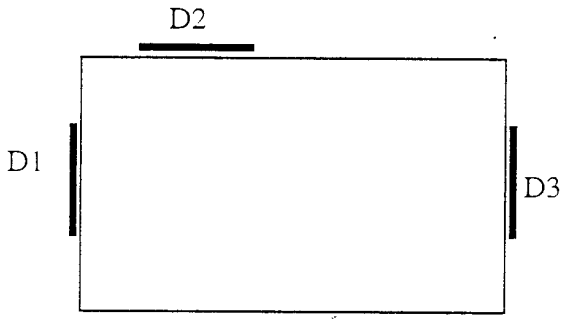

Figure 5. Arrangement of the three focal planes.

It is the use of off-axis parabolic M6 and M7 as final image relay and a cold-stop placed close to M6 which allows for the excellent image quality and the correction of the large image tilt, present in the system due to the curvature of the FIRST focal plane. The cost of this correction is a distorted image and a variable focal ratio. The distortion is illustrated in Figure 6, showing the image of a 5′ x 5′ object. Table 1 lists focal ratios for points A, B, and C in the FOV. Detector 1 behaves slightly better than the two others because the distance between M6 and M7 is shorter for this channel.

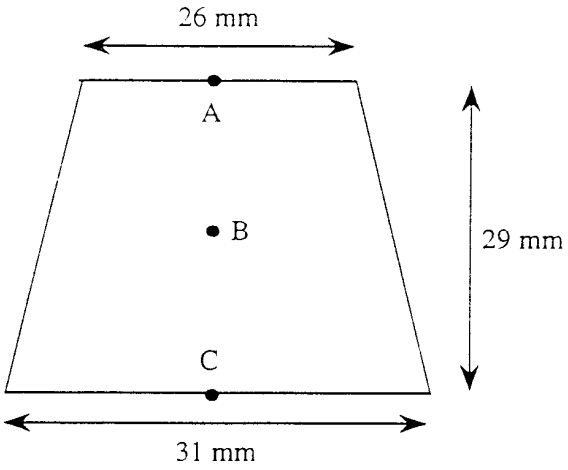

Figure 6. The image of a 5′ square object, illustrating the distortion of the final image. Points A, B, and C refer to Table 1.

Table 1. Tangential and sagittal focal ratios for the three points in the FOV named A, B, and C in Figure 1.

Point in FOV	Detector 1		Detectors 2 and 3	
	$F_{tangential}$	$F_{sagittal}$	$F_{tangential}$	$F_{sagittal}$
A (upper edge)	4.8	5.0	5.0	5.3
B (centre)	5.6	5.4	6.3	5.9
C (lower edge)	6.7	5.6	8.0	6.3

5. Conclusion

Optical design criteria and embryonic error budgets for the SPIRE photometer are presented. Comparison with the optical performance of the present baseline design indicates that it suffers from insufficient image and pupil quality. A new concept is proposed offering the required improvements. This is achieved at the cost of increased surface complexity and the introduction of distortion and variable focal ratio across the FOV. A scientific specification for the allowed variation in focal ratio is required in order to attempt a trade-off between scientific, optical, and mechanical performance.

20/11/98

Time sampling interferograms with an LVDT
Oversampling and interpolation

G.Michel
DESPA / MEUDON OBSERVATORY

1.1 Introduction :

This follows a previous report [1] on the evaluation of an LVDT transducer aimed at the sampling of long wavelength interferograms. Since the sampling accuracy we are looking for might be marginal with that kind of transducer it is important trying to improve it by oversampling and interpolation.

1.2 Experimental data available for the simulation :

This is based on the measurements performed on a prototype drive mechanism for CASSINI / CIRS available at Meudon. The drive is servoed around a 1cm scan LVDT position transducer.

This drive mechanism system has been characterized in term of position noise with a laser interferometer. The deviation from linearity has been recorded by time sampling the position. The number of samples recorded is about 16K for the 1cm range with a scan duration of 30 sec.

This file is then used for the simulation of 4cm range LVDT after multiplication of the deviation from linearity by a factor 3.5. This is to take into account the loss in sensitivity of the transducer going from 1 cm to 4 cm .

The simulation consists in generating the synthetic interferogram of a band pass filter in the spectral range 200-300 μm including the sampling errors. Then we evaluate the S/N in the spectrum.

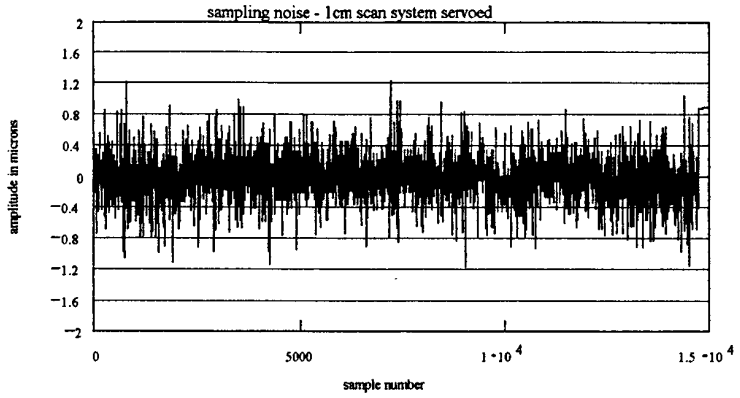

fig 1 :This is the position or jitter noise after compensation of the non-linearity. The value is .2 μm rms (scan length 1cm) . The corresponding file has been used for the simulation. For a 4 cm scan this jitter figure becomes .2 x 3.5 = .7 μm rms .

1.3 Oversampling the interferogram :

The interferogram produced is highly oversampled (factor 16) , its characteristics are :

double sided		
sample numbers	16	K (actual 15K)
spectral band	33.3 - 50	cm-1 (300 - 200 μm)
absorption line	41.7	cm-1
OPD	9.15	cm
sampling interval	6.1	μm
free spectral range	819	cm-1
resolution (no apodization)	.1	cm-1
scan duration	30	s
modulation frequency @ 33.3 cm -1	15.2	Hz
modulation frequency @ 50 cm-1	10.2	Hz

To verify the oversampling effect on the S/N, we split the 16K interferogram into 8 interferograms of each 2K samples. These interferograms are FFT transformed and apodized with a simple cosine window . The results are shown in the next figures .

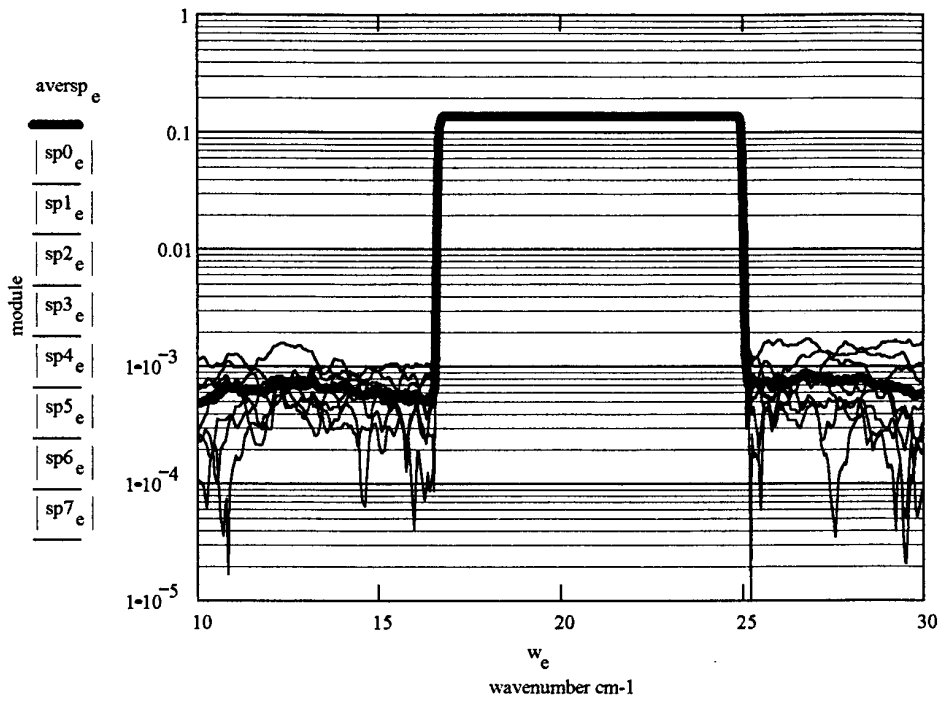

fig 2 : sp0..7 are the modules of the spectra of the 2K interferograms and aversp is the average of the 2K interferograms. The mean S/N of the spectra sp0..7 is 521 and that of the average of the 8 spectra is 992.

The oversampling by a factor 8 leads to an improvement of the S/N by 2 instead of 2.8 ($\sqrt{8}$) expected. This is of course the result of a single scan .The statistic would tend to $\sqrt{8}$ by considering multiple scans.

For the real handling of the interferograms we will proceed to the data compression with the following steps :

1/ numerical filtering to extract the spectral band of interest (33-50 cm-1).

2/ down-sampling the interferogram (by a factor 8 in the case of the previous simulation leading to a 2K interferogram).

In that case the S/N obtained with the 2K interferogram is identical to the S/N obtained by transforming directly the original 16K interferogram.

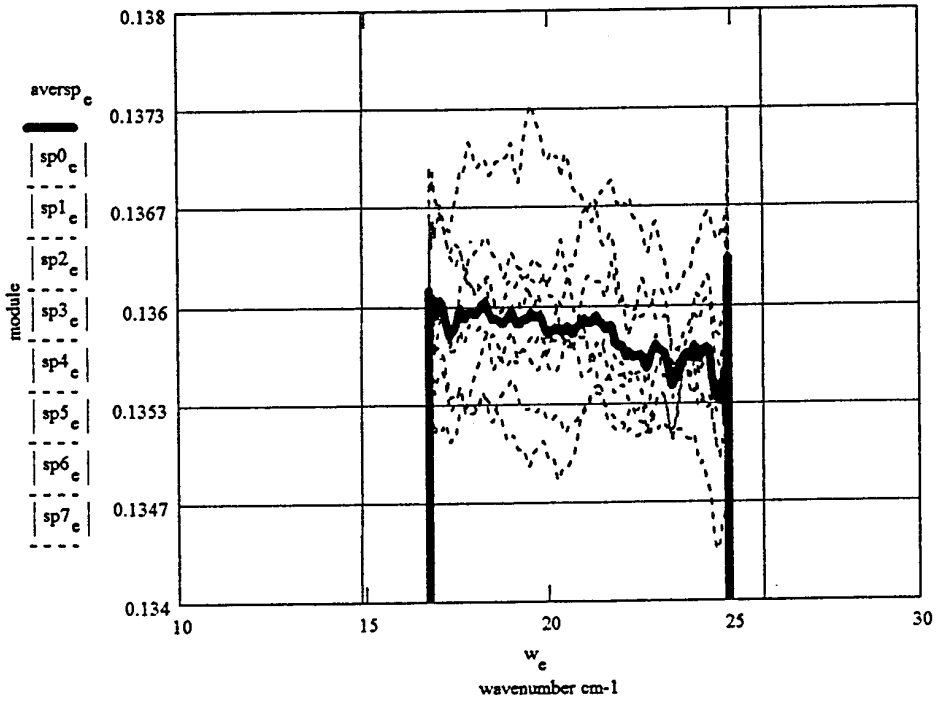

fig 3 : Same conditions as in the previous figure . The noise in the band pass is shown here with a linear scale.

As expected the oversampling improves significantly the S/N . For SPIRE the limitation will come from the data acquisition and real time processing load. At the moment a factor of 5 seems practical, leading to a potential $\sqrt{5}$ =2.2 factor improvement of the sampling accuracy.

The results of this simulation can be extrapolated for the different configuration of interferometer :

Michelson	Single Path	Single Path	Double Path
Interferogram	Double Sided	Single Sided	Single Sided
Oversampling factor	16	16	16
LVDT	4cm	2cm	1cm
Resolution (unapodized)	.1 cm-1	.1 cm-1	.1 cm-1
S/N	1000	2000	4000

1.4 Improvement of the accuracy by interpolation :

Interpolation could be an additional mean of reducing the sampling error in the case we have access the position [2]. This technique is illustrated in the next figure.

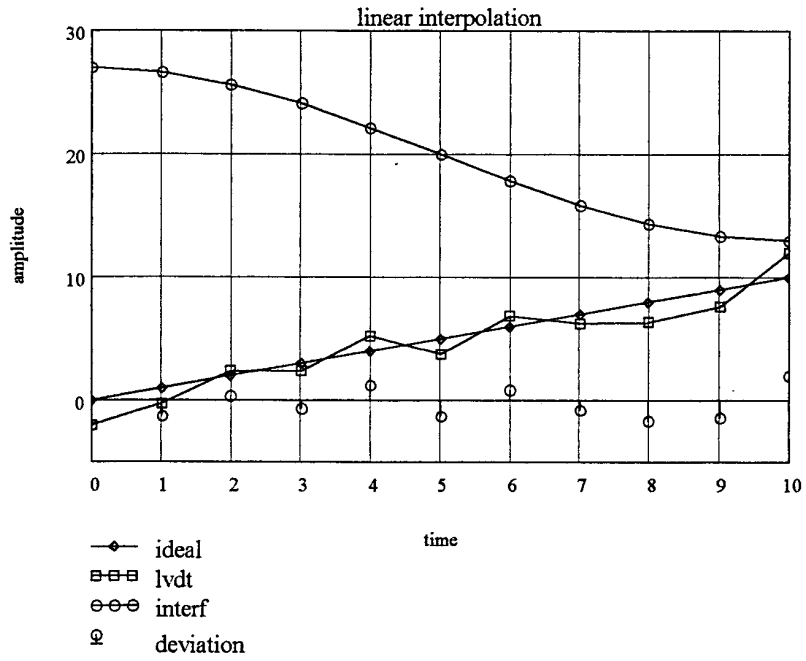

fig 4 : Principle of the interpolation. The curves shown are the interferogram, the ideal linear displacement, the lvdt actual position measurement and the deviation from ideal.
The correction consists in resampling the interferogram according to the amount of deviation from the ideal linear ramp.

To demonstrate this technique we can use the simulated interferogram and the sampling noise file and proceed to a simple linear interpolation which could be easily implemented in real time.
At this point, it is important to note that we have here a perfect correlation between the perturbated interferogram and the sampling noise.
In the real case the correlation factor might be low and that kind of correction useless (at the output of the transducer conditioner we have of course the information on the position plus electrical noise which is not related to the position).
Anyway what follows illustrate what we get with a correlation of 100 %.This gives an indication of the upper limit of the gain to be expected from that kind of interpolation.

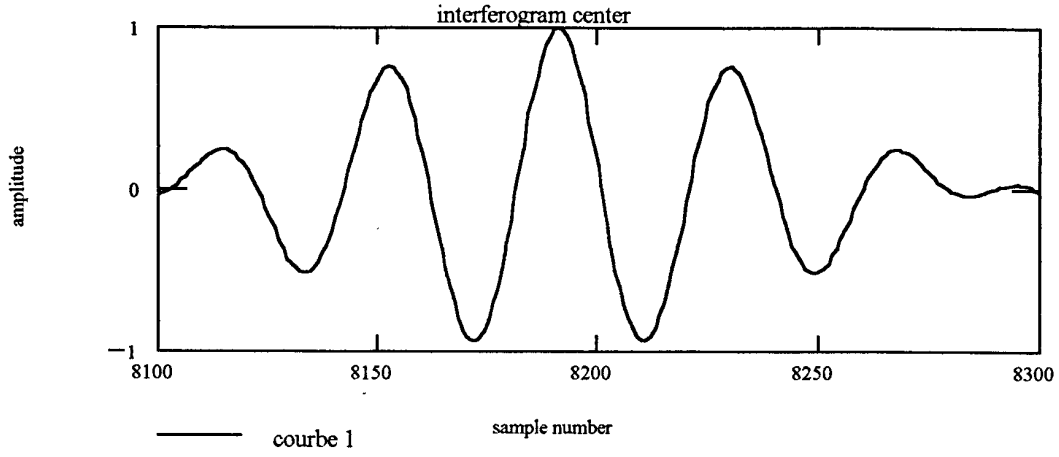

fig 5 : This is the center of the simulated interferogram including sampling errors. The error is more important at the center because since it is proportional to the derivative. This is shown in the next figure where we have the difference between the perturbated and ideal interferogram.

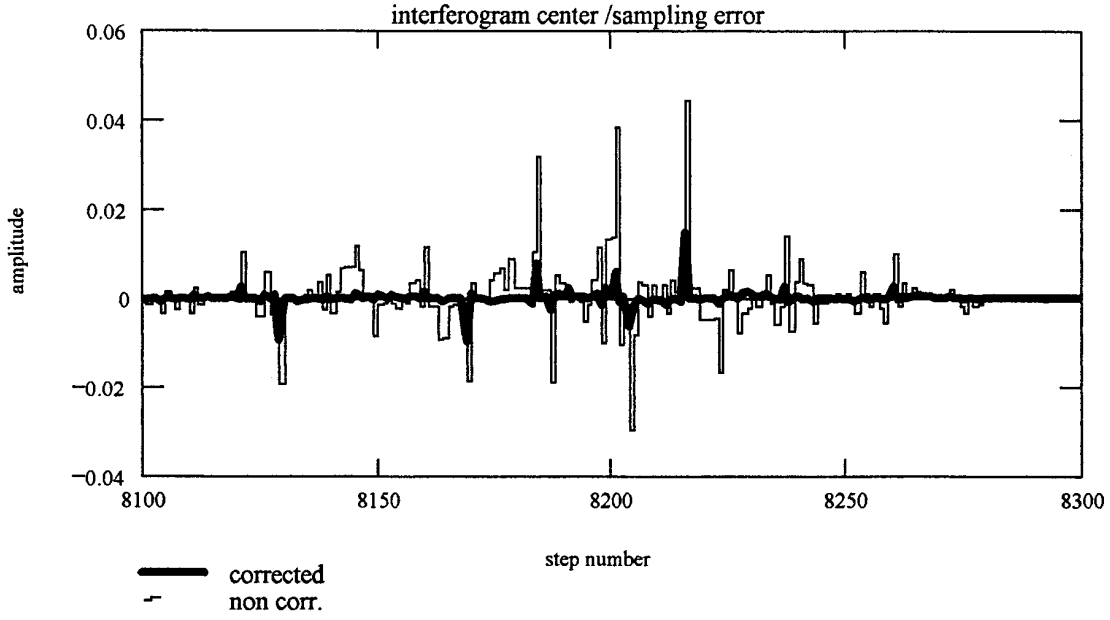

fig 6 : Here we can see the sampling errors of the non corrected and corrected interferogram. The improvement is quite significant.

Another way of showing the improvement is to compute the sampling noise over the free spectral range window.

$$wn_q := q \cdot \frac{fsr}{8192}$$

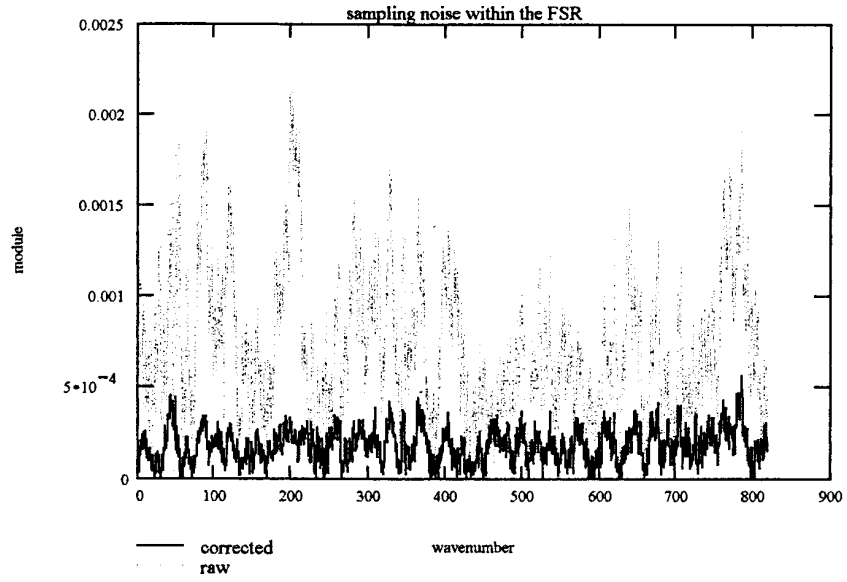

fig 7 :This shows the result of the sampling noise on the spectrum over the full spectral range with and without linear interpolation. There is a factor 4 improvement. This is the best we can get with a simple linear interpolation under the conditions of the simulation.

For the real case we can think of digitizing at the same time the interferogram and the LVDT output. It is probably equivalent to digitize the difference between the command ramp and the LVDT output i.e. the **error signal** (this will have the advantage of minimizing the dynamic range to get a good resolution with a 12 bits ADC).

The efficiency of that correction will depend on the degree of correlation between the **error signal** and the **actual jitter** as measured with the laser interferometer. To simulate this effect one can degrade the correlation index by adding white noise to the deviation from the ideal function cf (fig 4). The results are :

correlation index	S/N in the 33-50 cm-1 spectral range	gain factor corrected / non corrected
1	4108	4
.9	3045	3
.8	2451	2.4
.7	1971	1.9
.6	1600	1.5
.5	985	.9

This correlation measured on the CIRS prototype system is of the order of **.4** . Under this condition the interpolation would do more harm than good.

1.5 Conclusion :

As predictable, oversampling the interferogram is the very simple way of improving the sampling accuracy. As mentioned before the limitation will be the real time computation load. Altogether a factor 2 improvement over the jitter noise seems very realistic.

The interpolation can certainly be investigated on the prototype to be build. It seems that we will be strongly limited by the LVDT noise (the part non connected to actual displacement). In presence of vibrations the situation might be different and the interpolation become more effective.
At the moment the benefit of that kind of correction seems very unlikely.

1.6 **References :**

[1] G.Michel The sampling of interferograms with an LVDT transducer
Spire team meeting 15/5/98

[2] J.C. Brasunas and G.M. Cushman
Uniform time-sampling Fourier Transform Spectroscopy
APPLIED OPTICS / Vol. 36,No 10 / 1 April 1997